Publ. Astron. Obs. Belgrade No. 80 (2006), 367 - 375 *Poster*

INFLUENCE OF THE MAGNETIC FIELD ON THE VELOCITY OF THE HIGH FREQUENCY WAVES IN THE SOLAR CHROMOSPHERE

ALEKSANDRA ANDJIĆ[1,2] AND EBERHARD WIEHR[1]

[1] *Institut für Astrophysik, Friedrich-Hund-Platz 1, 37077 Göttingen, Germany*
E–mail: aandjic@yahoo.com

[2] *Prirodno Matematički Fakultet, Mladena Stojanovića 2, 78000 Banja Luka, Bosnia and Hercegovina*

Abstract. High frequency acoustic waves are thought to be the source of the mechanical heating of the chromosphere. The observed velocity interval of high frequency wave propagation starts with $3.7 \pm 0.4 \frac{km}{s}$ but the upper limit cannot be observed with the temporal resolution achieved in this work. Three areas of the Sun with the various activities are observed. Only events with the amplitudes larger than 50% of the maximum one were analysed in this work. The magnetic field has an influence on the propagation of high frequency waves. In the quiet Sun area only 49% of the observed events are connected with the magnetic field, while in areas with the magnetic structures 70% of the observed wave features are connected with the magnetic field.

1. INTRODUCTION

It is supposed that acoustic waves may be responsible for the energy transport to the chromosphere. The generation of those acoustic waves can be described by the 'Lighthill mechanism' (Lighthill, 1951). The application of this mechanism to the explanation of the solar atmospheric temperatures was developed in works which followed, (Stein, 1967; Stein and Leibacher, 1974). The theoretical models (Ulmschneider, 1971; Ulmschneider and Kalkofen, 2002; Ulmschneider, 2003) were taken as the starting point for this research.

The magnetic knots typically appear in dark intergranular lanes; and therefore they can be associated with the down-flow motions. So a suspicion arises that the magnetic field plays a role in the detected radial component of the group velocity of the high frequency waves.

The high frequency waves are detected in previous few decades (von Uexküll et al., 1985; Wunnenberg et al., 2003; Hansteen et al., 2000) and partially analysed

(Andic, 2005b), so a belief was formed that they are responsible for heating of the solar chromosphere.

2. OBSERVATIONS

Observations were done using the neutral spectral line Fe I 543.45nm, with the German Vacuum Tower telescope (VTT) on the Canary Islands, with the "Göttingen" Fabry-Perot spectrometer (Bendlin et al., 1992). The chosen line was a result of the initial presumption that only the acoustic waves appear in the quiet Sun areas, therefore there is no need to include the magnetic sensitive line and therefore to introduce an additional noise in the data sets.

The data sets, which were used in this work, had been taken during the observational campaign in 2004. The main objective was to achieve a repetition rate as fast as possible, allowing to study waves with shortest periods. Since the time evolution of high frequency waves was of main interest, reasonably long time sequences were taken. During the observations the adaptive optic was used, (Berkefeld and Soltau, 2001; Soltau et al., 2002).

Table 1: Dates, used lines and object of observation for obtained data sets.

mark	date	cadence[s]	object of observation
DS1	26.06.2004	22.7	quiet Sun
DS2	26.06.2004	22.7	pore
DS3	28.06.2004	29.9	G-band structures

Various cadences for the used data sets are caused by seeing. The more details of obtaining the data sets can be found in previous publications of one of the authors of this work (Andic, 2005ab). During observation campaigns the various solar regions were observed. The areas, which showed neither G-band structures nor other magnetic activities, were chosen as the Quiet Sun. For the active areas the field of view with the pores and with large number of G-band bright points was chosen.

The post focus instrument is made following the demands of the speckle reconstruction. Therefore it takes simultaneously two types of images, broadband and narrowband. The broadband images are images of the integrated light in the observed spectral line. The narrow band images are scanned through the spectral line by using the Fabry-Perot spectrometer.

3. DATA REDUCTION AND ANALYSIS METHODS

The data reduction for the broadband images is done with the program developed by P. Sutterlin following the method presented in works (de Boer et al., 1992; de Boer and Kneer, 1994).

The program set used for reconstruction of narrow band images was developed by Janssen (2003) and is based on a method presented in an earlier work (Keller and von der Lühe, 1992).

To reduce the contribution of the solar atmospheric fluctuation to the observed oscillation the velocity response functions were used. The velocity response functions for the spectral line Fe I 543.45nm and their calculation is the same as used in earlier works (Andic, 2005ab).

To form a time sequences, which were used for studying the time evolution, an additional correlation and de-stretching is done with the code described elsewhere (Yi and Molowny Horas, 1992), following the method introduced by another author (November, 1986).

Then, the wavelet analysis is applied with the Morlet wavelet as mother wavelet. The code for wavelet analysis (Torrence and Compo, 1998) was used as the base for our own code. The code is made for noncyclic data in the Fourier space. To avoid errors at the edges of the data set, apodisiation of the data was done before they are submitted to the wavelet analysis.

The result of the wavelet analysis is integrated over frequencies in an interval from the 22.3 mHz to 10mHz and subjected to the future analysis. It was necessary to determine the time shift and velocity of the observed wave packed component. A comparison of the power features with the granular events is done. The method is described in details in one of the previous paper (Andic, 2005b). To obtain information about the magnetic field we used the 'residual intensity effect', which indicated magnetic fields as reduced line depth (Chapman and Sheeley, 1977). The line used in this work is strong and since the 'residual intensity effect' increases with line strength (Stellmacher and Wiehr, 1979), one can expect such effects as presented in Fig. 4.

The continuum intensity is required to normalise the line profile for the determination of the 'residual intensity effect'. All profiles used in this work are normalised on the continuum intensity. Eq. 1 shows the expression used for the normalisation.

$$I_\lambda^{rel} = \frac{I_\lambda}{I_{cont}} \tag{1}$$

4. RESULTS

The wavelet analysis shows existence of the high frequency waves on the two observed heights. In our data set, the only velocity we were able to observe was the radial component of the group velocity of the observed high frequency wave packets. The results show differences among various objects of observations. The observed velocities in all the three data sets are within an interval from 3.4km/s to 18km/s. The upper limit is set with the temporal resolution of our data which was 22.7s, that leaves an open possibility of existence of even faster waves. In Fig. 1 the distribution of velocities in the analysed data sets is shown.

It is noticeable that the distribution is varying with the area of observation. When more magnetic structures are present in the area of observation, the faster waves have larger percentages. In this work only events with amplitude greater than 50% of the maximum one were observed.

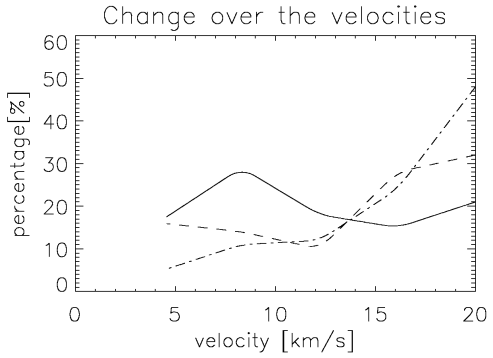

Figure 1: The distribution of velocities for the observed high frequency waves. The solid line presents the observed high frequency waves above the quiet Sun area, the dashed line above the area with G-band structures, and the dash-doted line above the pore.

Table 2: The overview of the percentage of the high frequency power features located over areas with the magnetic influence and those located above the areas without detectable magnetic influence.

velocities km/s	with residual intensity effect[%]	without residual intensity effect[%]
>19	70	30
17.6	38	62
8.79	61	39
5.87	39	61
4.4	37	63

4. 1. THE QUIET SUN

In the data set containing the quiet Sun as object of observation the most frequent time shift corresponds to a velocity of $8 \pm 0.7 \frac{km}{s}$, being close to the sound speed.

The observed velocities were tested for the magnetic influence with help of the 'residual intensity effect'.

Table 2 shows percentage variation for the velocity features located above the regions with the 'residual intensity effect'. In total, 49% of all registered power features are above the areas with the 'residual intensity effect'.

The solid line in the Fig. 2 presents the variation of the features of high frequency waves located above the areas with 'residual intensity effect'. It is observable that the percentage of the magnetic influence is larger with the faster waves. It is noticeable that there is less magnetic influence for the waves of 17.6km/s. Also a weaker magnetic influence is more frequent for the high frequency waves which cover larger spatial areas

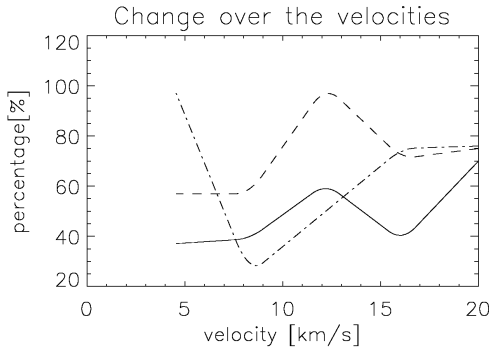

Figure 2: Distribution of the velocities for the observed high frequency waves above the areas where averaged line profiles show the 'residual intensity effect'. The solid line presents the observed high frequency waves above the quiet Sun area, the dashed line above the area with G-band structures, and the dash-doted line above the pore.

and the magnetic influence is stronger when the power feature covers a smaller spatial area. For the power features covering medium and small spatial areas and lasting over time intervals longer than 227s, the magnetic influence is evident.

4. 2. THE G-BAND STRUCTURES

For this part of analysis the two data sets are used, DS2 and DS3, since both of them have the G-band structures. For the data set DS2, from the field of view the part containing the pore and its surrounding was subtracted, and the rest was analysed as the dataset with the G-band structures.

For this data set, the most common are fastest waves, in the interval starting with a velocity of $17.6 \pm 0.4 \frac{km}{s}$, being more than double of the sound speed.

The distribution of velocities for these data sets is presented in Fig. 1 with the dashed line.

Table 3: The overview of the percentage of the high frequency power features located over areas with the magnetic influence and those located above the areas without detectable magnetic influence.

velocities km/s	with residual intensity effect[%]	without residual intensity effect[%]
>19	75	25
17.6	71	29
8.79	100	0
5.87	57	43
4.4	57	43

Out of all registered power features 71% are shown above the areas with the 'residual intensity effect'. The dashed line in Fig. 2 presents variations in the high frequency waves features located above the areas with the line gap effect. The waves with the observed velocities near the speed of sound have the biggest percentage of the events above the area with the magnetic influence.

4. 3. THE PORES

For this part the data set DS2 is used, taking in the consideration only the field of view that contained the pore and its surroundings.

Again, the most common are the fastest waves, within an interval starting with a velocity of $17.6 \pm 0.4 \frac{km}{s}$.

The distribution of velocities for these data sets is presented in Fig. 1, the dot-dashed line.

Table 4: The overview of the percentage of the high frequency power features located over areas with the magnetic influence and those located above the areas without detectable magnetic influence, for the data set with the pore in the field of view.

velocities km/s	with residual intensity effect[%]	without residual intensity effect[%]
>19	76	24
17.6	75	25
8.79	50	50
5.87	25	57
4.4	100	0

Out of all registered power features the 'residual intensity effect'. The dash-doted line in Fig. 2 presents variations of the high frequency waves features located above the areas with 'residual intensity effect'. Here the waves with the observed velocities near the speed of sound have the lowest percentage of the events above the area with the magnetic influence, while the rest of the velocities has a quite large percentage of the events above the areas with magnetic influence.

In this set of data there is around 10% of the events that have a 'negative residual intensity effect', example is visible on Fig. 3. These kinds of the events usually appear inside the pore itself.

5. DISCUSSION AND CONCLUSIONS

The data used for this work were obtained in (a) quiet solar regions, (b) active regions with G-band structures, and (c) active regions containing a pore, and it is found that these different objects of observation show substantial influences on the results. The high frequency waves travel through the chromosphere. This travelling seems to be highly complicated and affected by the magnetic field. For this analysis only power

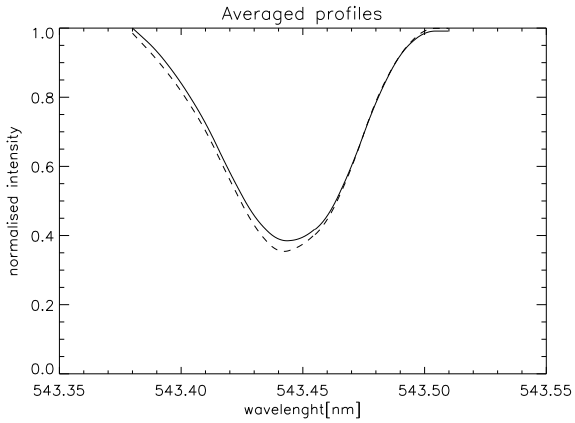

Figure 3: The averaged profiles normalised on the continuum intensity, which present the 'negative residual intensity effect'. The profile presented with the full line is one made over area of field where the investigated power feature covers around 4% of it. The profile presented by the dashed line is the averaged profile from the field of view where the investigated power feature covers 70% of the field of view.

features with the amplitude greater than 50% of the maximum one were analysed. The frequency range of the observed waves is from 22.3 mHz to 10mHz.

The highest percentage of the high frequency waves observed in the *quiet Sun* travels with the velocity of $8 \pm 0.6 \frac{km}{s}$, being close to the sound speed. Also a quite high percentage of the very fast waves appears in this data set, with a velocity that cannot be detected with our temporal resolution.

The events appearing in the area where the 'residual intensity effect' is noted have a percentage of 50%. Out of this the largest rate belongs to the fastest waves.

In the data sets with the *G-band structures* the waves tending to be fast, more than half noted events belong to the waves with velocities higher than 17km/s. Those waves appear above white-light structures that look like the G-band bright points. In more than 28% their velocity cannot be measured, since the changes in the power features seem to happen simultaneously at both heights, at the time resolution achieved in this work.

With the fraction of 71% events appear above the areas with the 'residual intensity effect'. The most unexpected result here is the large percentage of the events above the magnetic areas with the velocities closest to the speed of sound. The most of the events shows rather small 'residual intensity effect', while only 20% of events show a quite significant 'residual intensity effect', Fig. 4.

But since the stronger line should show the strong influence of the 'residual intensity effect', therefore all of them were taken into account.

The data set with *the Pore* shows a similar distribution of the observed velocities, including even their typical location. It is important to note, those events are rather rare above the pore itself, and tend to show only above visible internal structures of

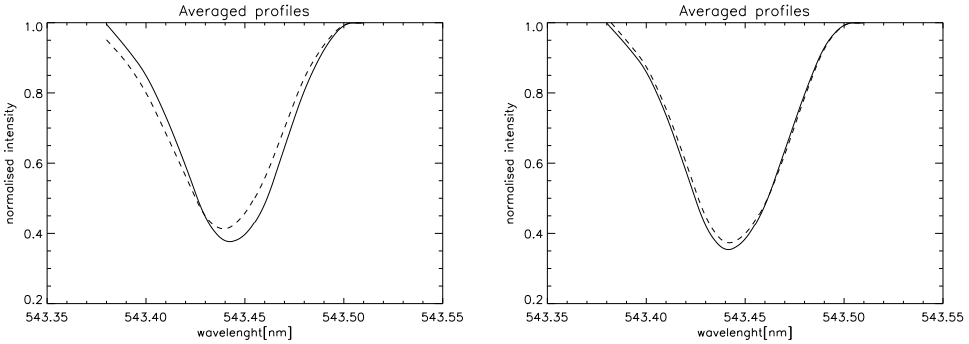

Figure 4: The averaged profiles normalised on the continuum intensity, which present the typical 'residual intensity effect' for the events closest to the speed of sound on both panels. The profile presented by the full line is one made over area of field where the investigated power feature covers around 4% of it. The profile presented by the dashed line is averaged profile from the field of view where the investigated power feature covers 70% of the field of view.

the pore. The percentage of the events appearing above the areas with noted 'residual intensity effect' is 69%. In this data set the magnetic influence appears almost equally often for all waves with the velocity which differs from the speed of sound. Also there is an interesting appearance of the 'negative residual intensity effect', appearing above the pore itself. The inner structure of the pore usually can not be resolved due to the exposure time. There is a possibility that 'negative residual intensity effect' is caused by one of those structures.

Acknowledgements. We wish to thank Dr. Sutterlin and Dr. Janssen for giving us software for data reduction. For the help with the observations we wish to thank Dr. Puschmann.

References

Andic, A.: 2005b, *SoPh*, submitted.
Andic, A.: 2005a, thesis, Göttingen university.
Bendlin, C., Volkmer, R., Kneer, F.: 1992, *Astron. Astrophys.*, **257**, 817.
Berkefeld, Th., Soltau, D.: 2001, Beyond Conventional Adaptive Optic, Venice.
de Boer, C.R., Kneer, F.: 1994, *IAUS*, **158**, 398D.
de Boer, C.R., Kneer, F., Nesis, A.: 1992, *Astron. Astrophys.*, **257**, L4-L6.
Chapman, G.A., Sheeley, JR., N.R.: 1977, *SoPh*, **51**, 61C.
Eibe, M.T., Mein, P., Roudier, Th., Fauronert, M.: 2001, *Astron. Astrophys.*, **371**, 1128.
Hansteen, V.H., Betta, R., Carlsson, M.: 2000, *Astron. Astrophys.*, **360**, 742.
Janssen, K.: 2003, Ph.D. Thesis, Goettingen University.
Keller, C.U., von der Lühe, O.: 1992, *Astron. Astrophys.*, **261**, 321.
Lighthill, M.J.: 1951, *Proceedings of the Royal Society*, A, **211**, p. 564.
November, L.J.: 1986, *Applied Optic*, 25, 3, 392.

Perez Rodrigues, E., Kneer, F.: 2002, *Astron. Astrophys.*, **395**, 279.
Soltau, D., Berkefeld, Th.,von der Luehe, O., Woeger, F., Schelenz, Th.: 2002, *AN*, 323,3 /4, 236.
Stein, R.F.: 1967, *SoPh*, **2**, 385S.
Stein, R.F., Leibacher, J.: 1974, *Astron. Astrophys.*, **12**, 407.
Stellmacher, G., Wiehr, E.: 1979, *Astron. Astrophys.*, **75**, 263.
Torrence, C., Compo, G.P.: 1998, *Bull. Amer. Meteor. Soc.*, **79**, 61.
von Uexküll, M., Kneer, F., Mattig, W., Nesis, A., Schmidt, W.: 1985, *Astron. Astrophys.*, **146**, 192.
Ulmschneider, P.: 2003, Lectures in Solar Physic, H.M. Antia, Springer Verlag.
Ulmshneider, P., Kalkofen W.: 2002, Dynamic Sun, B.N. Dwivedi, Ed., Cambridge University Press, 2003.
Ulmschneider, P.: 1971, *Astron. Astrophys.*, **14**, 275.
Wunnenberg, M., Kneer, F., Hirzberger, J.: 2003, *Astron. Astrophys.*, 271.
Yi, Z., Molowny Horas, R.L.: 1992, in: Proc. from LEST Mini-workshop, Software for Solar image processing, eds. Z. Yi, T. Daravann, R. Molowny Horas, Oslo ITA, 69.